Chapter 2

Metal Ion Exchange of N4Py in Cellular Systems

An extensive amount of work reported in literature has revealed that the nature of the metal coordinated to bleomycin can modulate its activity. This chapter presents the possibility for the ligand N4Py to undergo metal exchange and discusses the consequences for its biological activity.

A. Geersing
N. Ségaud
M. G. P. van der Wijst
E. Otten
M. G. Rots
G. Roelfes

2.1 Introduction

Bleomycins (BLMs), are a family of natural antibiotics produced by *Streptomyces verticillus*,[1] which are widely used as chemotherapeutic drugs to treat various types of cancer.[2] Coordination of a transition metal to its metal binding domain (*i.e.* Fe(II) or Cu(I)), results in formation of metallobleomycins that are able to react with dioxygen under reductive conditions,[3] causing significant oxidative damage to cellular organelles and molecules.[4–9]

Over time, BLMs have formed an inspiration for many metal polypyridyl complexes, of which the ligand *N,N*-bis(2-pyridylmethyl)-*N*-bis(2-pyridyl)-methylamine (N4Py) has arguably proven to be the most important. Since its discovery, N4Py has found multiple purposes in a wide range of scientific fields, and metal complexation with Mn(II),[10,11] Fe(II),[12–14] Co(II),[15] Ni(II),[16] Cu(II),[17] Zn(II),[17,18] Ru(II),[1819–21] and Pt(II)[22] has been reported. Of particular interest to our group is the biological activity of N4Py. The previously reported plasmid DNA cleavage activity of Fe(II)-N4Py complexes has been postulated to involve the formation of N4Py-Fe(III)-OOH by reaction with reactive oxygen species (ROS) such as $O_2^{\bullet-}$ and H_2O_2.[23–28] Additionally, N4Py-Cu-OOH,[29] N4Py-Mn(III)-O_2[29,30] and N4Py-Mn(IV)=O[31,32] species have been reported.

Previously, we have shown that Fe(II)-N4Py has a different mechanism of action in cells compared to BLM. Whereas BLM induces dsDNA breaks resulting in cell cycle arrest, N4Py was shown to induce apoptotic cell death.[33] As such, N4Py may be an interesting anti-cancer agent with appealing synthetic properties. Here, we investigated how the coordination of different first row transition metals could influence the activity of the N4Py molecule, both in cell-free systems as well as intracellularly. We show here that intracellularly, Fe(II), Cu(II) and Zn(II) complexes of N4Py can be formed, with the Fe(II) complex regarded as the most biologically active species. Our study clearly shows that the intracellularly active complex does not necessarily correspond with the initial treatment. Therefore, great care should be taken upon interpretation of biological studies involving metal complexes in general.

Some interesting knowledge regarding the biology of N4Py was obtained by Jackson and Kodanko, who showed that N4Py can effectively bind and mobilize Fe(II) from ferritin in aqueous solution.[34] In addition, Zuo et al. showed that N4Py can chelate Zn(II) ions, which can lead to inhibition of the X-linked inhibitor of apoptosis (XIAP) protein.[35] However, their conclusion that N4Py might also bind iron with a lower affinity than Zn(II) is in contrast to what we have found in the present study, as well

as contradictory to the zinc and iron dissociation constants (K_d) for N4Py that were measured and used in their own study.[34–36]

Extensive studies on BLMs in the past have indicated the importance of identifying the role of different metal species in the overall working of the drug *in vitro*. In cell-free systems, the activity of the metallobleomycins depends on the nature of the coordinated metal.[37–39] In these conditions, Fe(II)-BLM shows the highest DNA cleavage activity, whereas addition of excess Cu(II), Zn(II) or Co(II) to BLM in presence of Fe(II) completely abolishes its activity.[39,40] In contrast, studies in cell cultures show comparable levels of anti-tumor activity between the different metallo-BLMs (Zn(II), Cu(II), Fe(II)/(III)).[41,42] The comparable anti-tumor activity of the different metallo-BLMs may hint towards a common metallo-BLM that is generated intracellularly by metal exchange.[41,43] Even though BLMs have been studied for decades, the exact mechanism of action *in vitro* has yet to be fully elucidated. An advantage of N4Py compared to BLMs is that its compact structure facilitates the analysis of the chemistry that is involved in the biology of the complex, which provides more insight in the chemical entities that might be present in cells.

The goal of this study is to understand which metal complex of N4Py is mainly responsible for its biological activity in cells.

2.2 Results

2.2.1 Synthesis, Characterization and Metal Binding Studies

Metal complexes from the pentadentate ligand N4Py studied were synthesized following reported procedures (Supporting Information).[12,13,22,26,29,44] The complexes were isolated as perchlorate salts. In the case of Fe(III)-N4Py, the axial ligand (L) is a methoxy group, while a molecule of acetonitrile is coordinated in case of the other metals (Chart 1). Coordination of acetonitrile to Fe(III) results in its reduction to Fe(II), as previously described.[26] The crystal structures from the different N4Py metal complexes were compared (Figure S1) and bond distances, bond angles and other relevant crystallographic data are collected in Table S1. Some clear structural trends can be discerned. Firstly, the average bond distances of the four equatorial M-NPy bonds differ quite significantly, depending on the metal cation involved, with the average M-NPy bond lengths for the Mn(II) complex being 0.28 Å larger than for the iron(II) complex (2.251(8) Å over 1.971(8) Å respectively). The average trend in M-NPy bond distances being: Mn(II) > Zn(II) > Cu(II) ≈ Fe(III) > Fe(II). Secondly, the

position of the metal ion above the main plane of the four equatorial nitrogens differs, with Mn(II) showing the most distorted structure, being 0.55 Å out of plane, while Fe(II) shows the least distortion (0.21 Å). Finally, this out of plane distortion of the metal ion is also observed in the obtuse angle of N-M-N, with both nitrogen atoms being on opposite sides of equatorial plane. The smallest angle, for Mn(II)-N4Py, being over 16 degrees smaller than the largest one, for the Fe(II)-N4Py, with the general trend being the same as for the out of plane metal ion distortion. These findings altogether show that Fe(II) complexation with the N4Py ligand gives the least distorted octahedral complex, while Mn(II) complexation results in the formation of the most distorted octahedron. This suggests that Fe(II) is structurally the best suited metal ion for N4Py.

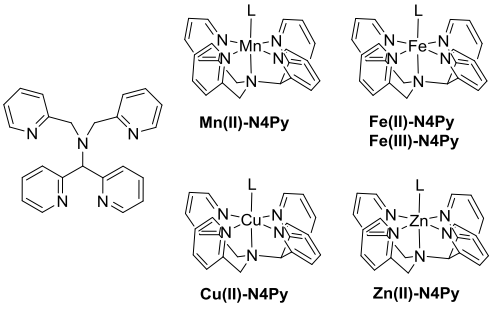

Chart 1. Structure of the ligand N4Py and its metal complexes.

In order to obtain spectroscopic data to support the results obtained in the cell culture studies (*vide infra*), the composition and conditions of the cell culture medium were simulated as much as possible (Supporting Information). The N4Py metal complexes were dissolved in PBS (pH 7.4, 37 °C) and their intrinsic UV/vis and electrochemical properties were analyzed (Figure 1, Table S2). All complexes showed pyridyl centered ligand π-π* charge transition bands between 200 and 300 nm. The absorption spectrum for Mn(II)-N4Py indicated an additional small shoulder band around 320 nm (400 cm^{-1} M^{-1}). Furthermore, cyclic voltammograms show a Mn(III/II) irreversible oxidation peak at E_{pa} = 0.7 V vs Ag/AgCl.[10] The Fe(II)-N4Py complex showed two clear absorption bands at 377 nm (2 000 cm^{-1} M^{-1}) and 460 nm (1 450 cm^{-1} M^{-1}), assigned to metal to ligand charge transfer (^{1}MLCT) transitions.[14] An irreversible Fe(III/II) oxidation peak was observed at E_{pa} = 0.18 V vs Ag/AgCl. Correspondingly, the ferric iron complex showed a similar oxidation peak, and had a near-UV absorption band at 370 nm (>2 500 cm^{-1}, M^{-1}).[26] For Cu(II)-N4Py, a broad

absorption band centered at 905 nm (170 cm^{-1} M^{-1}) and a higher energy shoulder around 730 nm (100 cm^{-1}, M^{-1}) were observed. CV data showed a reversible Cu(II/I) oxidation peak at E_{pa} = -0.42 V vs Ag/AgCl which is in accordance with what has previously been reported.[30] The zinc coordinated complex is spectroscopically silent, although its voltammogram shows the disappearance of the irreversible ligand oxidation peak at 1.02 V vs Ag/AgCl,[45,46] which evidences the binding of Zn(II) to N4Py (Figure S2). This is supported by pronounced changes in ^{1}H-NMR chemical shifts in comparison to the ligand N4Py (Supporting Information).

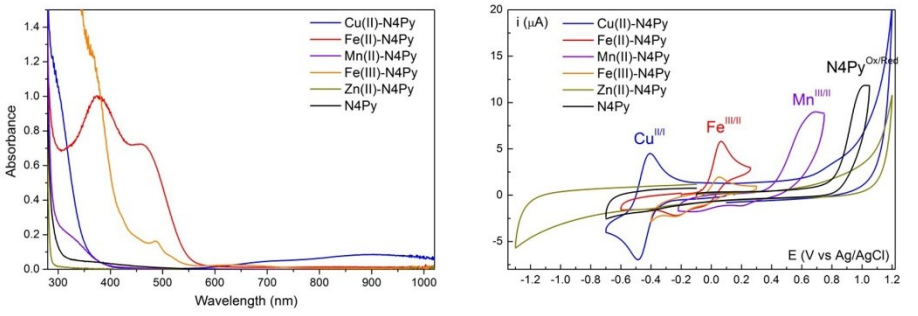

Figure 1. UV/vis absorption spectra (top) and cyclic voltammograms (bottom) of the N4Py metal complexes (0.5 mM) in PBS (pH 7.4, 37°C) under an argon atmosphere.

Since it was shown that N4Py can form complexes with all investigated metals, we were interested to see whether N4Py was able to bind these bioavailable metals under cell free conditions. The spectra and voltammograms of the solutions containing N4Py:metal 1:1 ratios are shown in Figure 2. Under the indicated conditions, N4Py seems to coordinate readily to Zn(II), Cu(II) and Fe(II) while coordination is limited for Mn(II) and almost non-existing for Fe(III).

Addition of Fe(II) solution aliquots to N4Py solution resulted in the progressive disappearance of the ligand oxidation peak (Figure S2) and simultaneous formation of the Fe(III/II) oxidation peak. In addition, Fe(II) addition resulted in almost immediate appearance of its typical ^{1}MLCT bands. A maximum conversion to the iron complex of 74 % was observed ($t_{1/2}$ = 15 s and k = 0.12 s^{-1}, Figure S3 and Table S3). Contrary to Fe(II), addition of Fe(III) to N4Py did not result in formation of a CT band in the absorbance spectrum, nor did it result in extinction of the ligand oxidation peak or formation of an Fe(II)/Fe(III) peak in the voltammograms. Addition of Mn(II) to N4Py resulted in limited coordination to N4Py, indicated by only partial disappearance of the irreversible ligand oxidation peak in combination with the broad

peak corresponding to the Mn(III/II) couple. Addition of Cu(II) to the ligand resulted in full disappearance of the ligand oxidation peak and appearance of the Cu(II/I) oxidation peak. However, formation of the broad absorption band around 900 nm (160 cm^{-1} M^{-1}) showed a maximum conversion of 50 % ($t_{1/2}$ = 30 s and k = 0.066 s^{-1}, Figure S3, Table S3). Addition of Zn(II) to N4Py resulted in full disappearance of the ligand oxidation peak, suggesting that the Zn(II)-N4Py complex is readily formed.

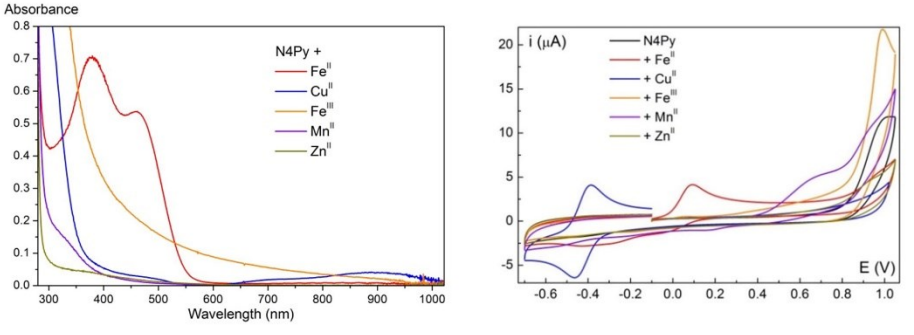

Figure 2. UV/vis absorption spectra (top) and cyclic voltammetry spectra (bottom) after stoichiometric addition of metal perchlorate salts to the N4Py ligand (0.5 mM) in PBS (pH 7.4, 37°C) under an argon atmosphere.

In view of a cellular environment, it is important to know whether exchange of Fe(II) with other biologically available metals can take place if the Fe(II)-N4Py complex is present in the cell. Absorption spectra suggest that a mixture of Fe(II) and Cu(II) complexes can be present in cells. The kinetic curves show that in the presence of Mn(II), Fe(III) or Zn(II) , no metal exchange occurs (Figure 3). Once the Fe(II)-N4Py complex is formed, it is therefore favored over the Mn(II), Fe(III) and Zn(II) complexes. In contrast, in the presence of Cu(II), a conversion of 70 % from Fe(II)-N4Py to Cu(II)-N4Py occurred. A process that is slow compared to Cu(II) binding to N4Py ($t_{1/2}$ = 2.5 min, k = 0.0051 s^{-1}, Table 1, Figure S4).

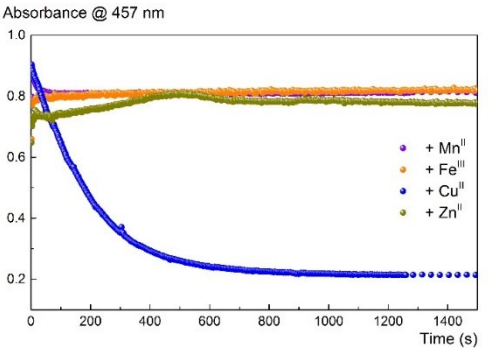

Figure 3. Evolution in time of the Fe(II)-N4Py ^{1}MLCT band at 457 nm in the presence of different metal ions. The kinetic curves were obtained by adding stoichiometric amounts of metal salts to a solution of Fe(II)-N4Py.

Table 1. Conversion of metal-N4Py complexes by addition of metal salt with indicated conversions at t = 1500 s, half-times and rate constants. Left: conversion of Fe(II)-N4Py to the metal N4Py complexes of the indicated metal ions. Right: conversion of the indicated N4Py complexes to Fe(II)-N4Py upon addition of an Fe(II) metal salt.

Metal salt	Conv. to metal complex	$t_{1/2}$ (min)	k (s^{-1})	Metal complex	Conv. to Fe(II)-N4Py	$t_{1/2}$	k (s^{-1})
Mn(II)	0 %	-	-	Mn(II)-N4Py	57 %	57 s	0.12
Fe(III)	0 %	-	-	Fe(III)-N4Py	100 %	10 s	0.24
Cu(II)	70 %	2.5	0.0051	Cu(II)-N4Py	39 %	33 s	0.028
Zn(II)	0 %	-		Zn(II)-N4Py	44 %	10 min	0.00084

Although Fe(II) was shown to exhibit the best metal binding to N4Py, it has to be considered that other metal complexes could also be present in cells after incubation with N4Py. We thus studied the ability of Fe(II) to exchange with the different metals coordinated to N4Py, by following the formation of the ^{1}MLCT band at 457 nm in time (Figure 4, Table 1). In general, once N4Py coordinates to a bioavailable metal other than Fe(II), it is able to exchange its coordinated metal with Fe(II) in the order: Fe(III) > Mn(II) > Zn(II) > Cu(II), a trend that, for the divalent ions, seems consistent with the Irving-Williams series.[47] Mn(II) appeared to give the most labile complex and Zn(II) the least.

Addition of Fe(II) to a solution of Fe(III)-N4Py resulted in fast and complete conversion to the Fe(II) complex, again suggesting the Fe(II) complex is completely favored over its Fe(III) analogue. Note, however, that the conversion might be ascribed to electron transfer, as opposed to actual physical exchange of metal ions. In the case of Mn(II)-N4Py, a majority of Mn(II) is exchanged by Fe(II) at a similar rate as for Fe(II) binding to N4Py ($t_{1/2}$ = 57 s, k = 0.12 s^{-1}, Figure S5) which indicates that binding of Mn(II) to N4Py is very labile, and addition of Fe(II) leads to a more stable product. Significant conversion of the Cu(II)-complex is observed (39 %), albeit with much slower kinetics than for Mn(II) ($t_{1/2}$ = 33 s, k = 0.028 s^{-1}). Importantly, conversion of Cu(II)-N4Py to form Fe(II)-N4Py is about five times faster than the opposite scenario. This indicates that both Fe(II) and Cu(II) are quite inert in the N4Py environment, with a slight kinetic preference for Fe(II)-N4Py. However, depending on the relative concentrations of the metal ions, a mixture of both complexes will thus most likely be present in cells. The Zn(II)-complex seems quite stable under the indicated conditions: even though almost half of the complex gets converted to the Fe(II) complex (44 %), the kinetics are very slow ($t_{1/2}$ = 10 min, k = 0.00084 s^{-1}). This suggests that the Zn(II) is the least labile of the studied metals in the N4Py environment.

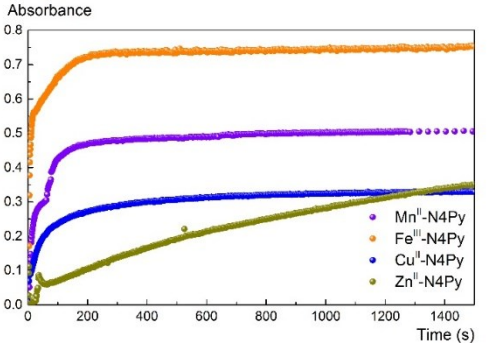

Figure 4. Evolution on time of the ^{1}MLCT at 457 nm after addition of Fe(II) to solutions of N4Py metal complexes.

2.2.2 DNA Cleavage

Since various metals can bind to N4Py in PBS buffer (pH 7.4, 37 °C), it is important to study the differences in biological activity of the five N4Py metal complexes studied herein. Their DNA cleavage activities were determined by using supercoiled pUC18 plasmid DNA at 37 °C in the presence of dithiothreitol (DTT). Gel analysis after 30

min incubation showed almost complete disappearance of supercoiled DNA in the presence of Fe(II)- and Fe(III)-N4Py, while the other complexes did not show any significant amount of DNA cleavage (Figure 5a). The average number of single-strand cuts per DNA molecule (*n*) was calculated from the amount of nicked and linear DNA formed. (Figure 5b, for equations see Supporting Information) Clearly, the Fe(II) and Fe(III) complexes caused the largest amounts of single-strand cuts (5.5 ±0.3 and 4.8 ±0.3 cuts, respectively), with almost all supercoiled DNA consumed within 30 min. Evidently, in the case of Mn(II), Cu(II) and Zn(II), very little cleavage activity was observed (<0.3 cuts), indicating their almost negligible activity in cell-free systems.

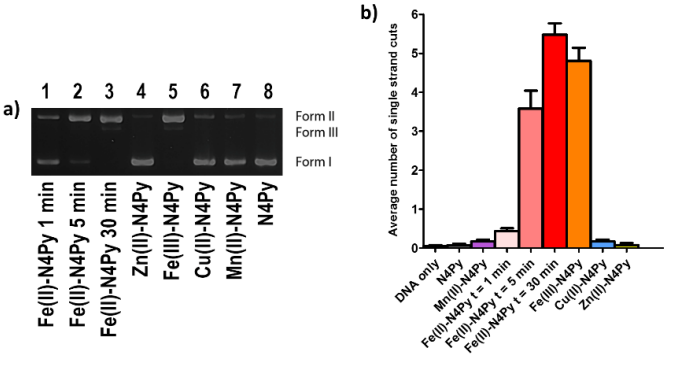

Figure 5. (a) Gel analysis of the cleavage of supercoiled DNA (Form I) to give nicked DNA (Form II) and linear DNA (III) in Tris-HCl (pH 8.0) at 37 °C after 30 min (with exception of lanes 1 and 2). Concentrations used: 1.0 μM complex, 0.1 μg μl-1 pUC18 plasmid DNA (300 μM in base pairs) and 1.0 mM DTT (b) Average number of single-strand cuts per DNA molecule (n). Error bars represent the uncertainty limits of the data, based on a Monte Carlo simulation, taking into account a standard deviation σ of 0.03 of the individual DNA fractions. A correction factor of 1.31 was used to compensate for the reduced ethidium bromide uptake capacity of supercoiled DNA.

2.2.3 Cell Studies

The mitochondrial metabolic activity of N4Py complexes was evaluated by the MTS assay.[48,49] Two cancer cell lines (A2780, SKOV3) and a non-cancerous cell line (OSE-C2) were chosen for this study. Cells were treated for 24h with different concentrations of N4Py and its metal complexes. The IC_{50} values for all cell lines were found to be in the range of 5-10 μM for N4Py, Mn(II)-N4Py, Fe(II)-N4Py and Fe(III)-N4Py (Figure 6, Table 2). Notably, an unexplained, sudden transition from high to almost no cell viability was observed for these compounds within this concentration range. This observation was in agreement with the cell viability as assessed by light

microscopy. The IC_{50} values for Cu(II)-N4Py lie around 50 µM, and treatment with Zn(II)-N4Py resulted in hardly any cellular damage (IC_{50} > 50 µM). We thus observe the highest activity for Fe(II)-, Fe(III)- and Mn(II)-N4Py, with little specificity towards cancer cells, compared to non-cancerous cells.

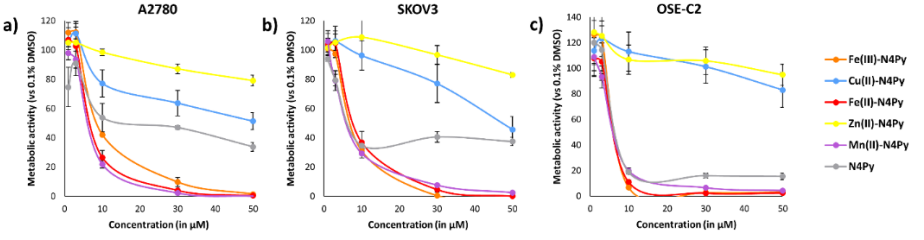

Figure 6. Metabolic activity (MTS assay) upon treatment with N4Py metal complexes. Cells were treated for 24 h with 1, 3, 10, 30, 50 µM N4Py and N4Py metal complexes. Experiments were conducted three times. Within each treatment, each treatment was measured three times. Data are presented as the mean ± SEM.

Table 2. Metabolic activity upon treatment with N4Py metal complexes displayed as IC_{50} values.

	A2780 (µM)	SKOV3 (µM)	OSE-C2 (µM)
Mn(II)-N4Py	9 (± 3)	6 (± 0)	6 (± 0)
Fe(II)-N4Py	10 (± 4)	8 (± 1)	6 (± 0)
Fe(III)-N4Py	11 (± 3)	7 (± 0)	6 (± 0)
Cu(II)-N4Py	≈ 50	≈ 50	≈ 50
Zn(II)-N4Py	> 50	> 50	> 50
N4Py	17 (± 8)	6 (± 0)	6 (± 1)

It is known that the MTS assay can suffer from interfering processes.[50–56] In addition, since the decrease in metabolic activity can be explained by either cytotoxic or cytostatic processes, a propidium iodide PI/FACS assay was performed. Cells will only stain PI positive once the cell membrane becomes permeable, i.e. when cells are late apoptotic or necrotic. The PI assay was performed by treating cells for 24 h with 10 µM of the metal complexes (Figure 7), as this was the lowest concentration where clear differences between the different metal complexes became visible (Figure 6). The Cu(II)- and Zn(II)-N4Py complexes showed the lowest cytotoxicity (5-

10 %), which correlates with their minor effect on metabolic activity. Conversely, Mn(II)-, Fe(II)-, Fe(III)-N4Py showed significant amounts of cell death, ranging from 56 % to 96 %. Likewise, the N4Py ligand, in the absence of coordinated metal ion, appeared to be the most toxic compound in all three cell lines, with cell death levels varying from 79 % (± 1.8) in A2780 up to 96 % (± 0.5) in OSE-C2 cells. Based on the cell-free experiments, the cytotoxicity is expected to be induced by an N4Py metal complex and not by the ligand alone. Therefore, this result suggests that the N4Py ligand is able to bind metals in the cellular environment. The combined data of Figure 6 and Figure 7 clearly indicates that the decrease in metabolic activity was caused mainly by a cytotoxic effect.

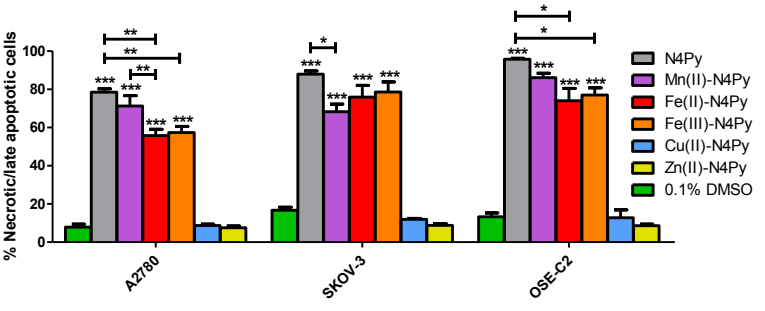

Figure 7. Cytotoxicity upon treatment with N4Py metal complexes. Cell death was determined in A2780, SKOV3 and OSE-C2 cells treated for 24 h with 10 µM N4Py and its metal complexes (Mn(II), Fe(II), Fe(III), Cu(II), Zn(II)). Cells were stained by propidium iodide (PI) and the percentage of late apoptotic/necrotic cells was analyzed by FACS. Data are presented as the mean ± SEM from three independent experiments. *** P < 0.001; ** P < 0.01; * P < 0.05.

The known oxidative mechanism of DNA cleavage in cell free systems by Fe(II)-N4Py and the reported oxo-species of the manganese, iron and copper N4Py complexes (*vide supra*) together with the strong cytotoxicity of N4Py in cells, raised the question whether the cytotoxicity of the metal N4Py complexes is a result of excessive ROS formation in the cells. In order to determine the intracellular hROS formation upon treatment of A2780 cells with the N4Py ligand and its metal complexes, the hROS probe APF was selected (Figure 8).[57] Treatment of A2780 cells with N4Py gives a twofold (2.1 ±0.1) increase in fluorescence of PI versus 0.1% DMSO control. This suggests that N4Py can enter the cell and bind transition metal ions to form complexes able to generate hROS. The complex Zn(II)-N4Py did not show any ROS formation, which is in agreement with its redox inactive nature. Since exchange of Zn(II) for Fe(II) seems to be very slow, this finding suggests that little of the Fe(II)-

N4Py complex is actually formed in cells. In the presence of the other complexes, the amount of ROS increased between 1.6 to 2.3 fold with respect to DMSO.

To verify that the APF probe indeed detects the formation of hROS produced by the N4Py metal complexes, cells were co-treated with the antioxidant precursor N-acetylcysteine (NAC). It is generally believed that NAC protects cells from oxidants both directly, as a scavenger of free radicals, and indirectly, as a precursor for GSH.[58–60] Upon co-treatment with NAC, the hROS production of cells treated with N4Py and all N4Py metal complexes was completely abolished, except for Cu(II)-N4Py (Figure 8). Remarkably, the hROS formation was almost doubled from 1.9x to 3.3x versus 0.1% DMSO upon co-treatment of Cu(II)-N4Py with NAC. This finding likely indicates the interaction of Cu(II) with the antioxidant, resulting in strongly elevated ROS levels (*vide infra*).

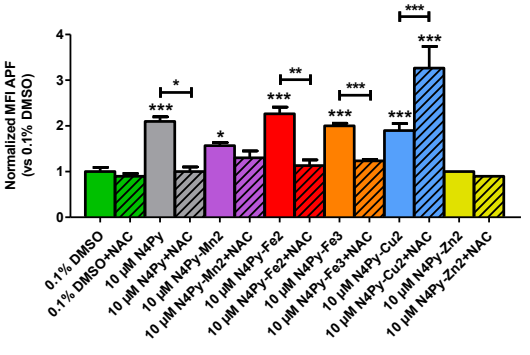

Figure 8. hROS formation upon treatment with N4Py metal complexes. A2780 cells were treated for 24 h with the N4Py ligand, its metal complexes, or solvent control. The dashed columns represent the results obtained by co-treating with 5 µM of the antioxidant precursor N-acetylcysteine (NAC). hROS formation was detected by the ROS probe APF. Flow cytometric analysis of APF emission was used to obtain the mean fluorescent intensity (MFI) for each condition. The MFI was normalized to solvent control (green). Every experiment was carried out three times. Each bar shows the mean ± SEM. *** P < 0.001; ** P < 0.01; * P < 0.05.

These results clearly revealed the increase of hROS levels in A2780 cells treated with N4Py and its metal complexes. In order to determine whether the cytotoxicity as observed in Figure 7 is hROS-dependent, the PI/FACS assay was repeated in the presence of two types of antioxidants: NAC or L-ascorbic acid 2-phosphate (AA2P)[61,62] (Figure 9 and Figure S6). The level of cell death induced in the different cell lines (A2780, SKOV3, OSE-C2) was comparable for each treatment. Interestingly, the presence of NAC or AA2P does not seem to impact the amount of cell death

when cells are treated with N4Py or Mn(II)-N4Py. Contrary, the co-treatment with NAC completely abolished the cell death induced by the iron N4Py complexes, with a clear effect of AA2P as well. Furthermore, the presence of NAC in the Cu(II)-N4Py treated cells resulted in an extreme increase in cell death (up to 100% in A2780), indicating that reduction of Cu(II) to Cu(I) by NAC not only induces hROS production by reaction with dioxygen, also, it induces high amounts of cell death. As expected, treatment with non-complexing AA2P had no effect on ROS formation by Cu(II)-N4Py. Likewise, Zn(II)-N4Py treated cells showed no significant response to the co-treatment with neither NAC nor AA2P.

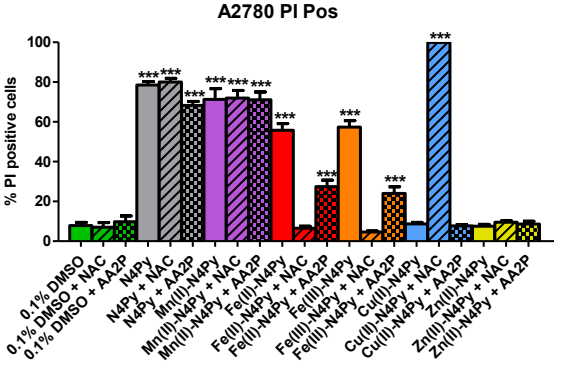

Figure 9. The effect of antioxidants on the N4Py metal complex-induced cytotoxicity. Cell death was determined in A2780 cells treated for 24h with 10 µM N4Py and its metal complexes (Mn(II), Fe(II), Fe(III), Cu(II), Zn(II)). Dashed and squared columns show cells co-treated with 5 µM N-acetyl cysteine (NAC) or 16 h pre-treated and co-treated with 173 µM L-ascorbic acid 2-phosphate (AA2P), respectively. Cells were stained by propidium iodide and the percentage of late apoptotic/necrotic cells was analyzed by FACS. Data are presented as the mean ± SEM from three independent experiments. *** $P < 0.001$; ** $P < 0.01$; * $P < 0.05$.

The ability of the different complexes in inducing oxidative DNA damage in living cells was studied. The extent of double strand DNA break (DSB) formation was determined using flow cytometric detection of phosphorylated histone H2AX (γH2AX).[63] The histone protein H2AX forms a key component in DNA repair, since it becomes rapidly phosphorylated at serine 139 and accumulates at emerging DSB sites.[64,65] After a 24h treatment with 30 µM of N4Py and its metal complexes, the percentage of γH2AX positive cells was determined in SKOV3 cells (Figure 10). Interestingly, all reagents showed significantly higher γH2AX levels compared to the solvent controls ($P < 0.001$), which indicates that at this concentration, nuclear DNA

damage is induced by treatment with N4Py and all of the metal complexes. The Fe(II) complex appears to produce slightly more dsDNA damage compared to the five other reagents ($P < 0.001$ against Mn(II)-, Cu(II)-, and Zn(II)-N4Py; $P < 0.01$ against N4Py and Fe(III)-N4Py). An order in decreasing dsDNA break efficiency can be given: Fe(II)-N4Py > N4Py ≈ Mn(II)-N4Py ≈ Fe(III)-N4Py > Cu(II)-N4Py ≈ Zn(II)-N4Py.

DSBs can be caused by various factors. Some reagents create DSBs directly, such as BLM and doxorubicin,[63,65] while other factors such as ROS formation, metabolic processes, deficient DNA repair mechanisms, telomere erosion and programmed cell death, such as apoptosis, can also play a significant role.[66] In order to address the contribution of apoptosis in the induction of DSBs by N4Py and the N4Py metal complexes, SKOV3 cells were treated with the broad range caspase-inhibitor carbobenzoxy-valyl-alanyl-aspartyl-[O-methyl]-fluoromethyl-ketone (ZVAD-FMK). Fluoromethylketones (FMKs) are irreversible inhibitors of cysteine proteases such as those of the caspase family by means of alkylation of the active-site thiol.[67] Upon addition of ZVAD-FMK, a significant reduction of 46 to 57 % in γH2AX levels was observed for all compounds except Zn(II)-N4Py (Figure 10). This result revealed that about half of the observed dsDNA damage was the result of apoptosis induced by N4Py or metal complexes. Nevertheless, even after inhibition of the caspase-dependent apoptosis pathway, the amount of observed dsDNA damage was still significant for all reagents ($P < 0.05$ for Cu(II)-N4Py, $P < 0.001$ for N4Py, Mn(II)-, Fe(II)-, Fe(III)- and Zn(II)-N4Py), indicating that other cell death mechanisms are also involved.

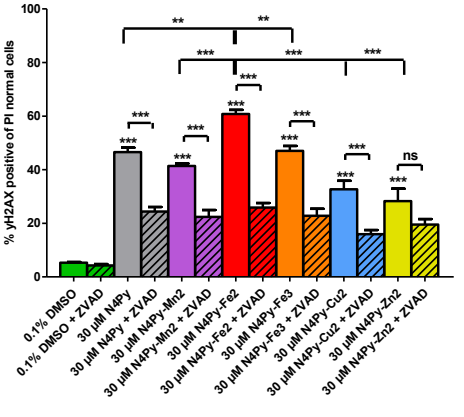

Figure 10. Double strand DNA damage (γH2AX) in non/early apoptotic cells induced by the N4Py metal complexes. SKOV3 cells were treated for 24 h with 30 µM N4Py and its metal

complexes. FACS analysis of γH2AX was used in combination with propidium iodide (marker for DNA content), to exclude late apoptotic cells (subG1 peak) from analysis. Co-treatment with 20 μM of the pan-caspase inhibitor zVAD-FMK could reveal the contribution of apoptosis to the total dsDNA break induction. The gate for γH2AX positive cells in solvent control was set at 5 %. Each value represents mean ± SEM from three independent experiments. ***P < 0.001; **P < 0.01; ns, not significant.

2.3 Discussion

In this study, we described how different metals can affect the intracellular properties of the synthetic BLM-mimic N4Py. These findings presented here have encouraged us to come up with the following hypothesis (Scheme 1): we propose that the active complex that causes oxidative damage to the cell is the Fe(II)-N4Py complex, which therefore can differ from the complex that was initially added to the cell culture medium, that is, it is irrespective of the initial metal ion coordinated. For this, we have the following arguments: (i) In cell-free systems, Fe(II)-N4Py is the only complex that possesses oxidative DNA cleavage activity. In contrast, *in vitro*, all N4Py metal complexes can generate DSBs, albeit with different efficiencies; at one end of the scale we have Fe(II)-N4Py being the most efficient, and on the other end, we have Cu(II)-N4Py and Zn(II)-N4Py being the least efficient. We showed that at least part of these DSBs are directly generated by the N4Py metal complex itself, whereas the remaining are indirectly generated, i.e. via the induction of apoptosis. This is in line with our previous *in vitro* observations for the Fe(II)-N4Py complex.[33] (ii) It is proposed that the observed oxidative damage can be in part subscribed to direct oxidation by the iron N4Py complex, which seems to be the only complex of N4Py that is strong enough to oxidize cellular components, such as DNA. Even though formation of an N4Py-Cu-OOH species has been reported,[29] it was found to be a sluggish oxidant. Similarly, many Mn-oxo complexes show much less reactivity in oxidation reactions than their Fe-oxo counterparts.[68] Since coordination of Mn(II) to N4Py does not appear to be favorable and Mn(II) is readily exchanged for Fe(II), it is likely that mainly metal exchange, forming the Fe(II)-N4Py complex, is responsible for the observed intracellular activity. In addition, since the chemistry of Zn(II) is driven by s-electrons instead of d-electrons, it is essentially not redox active under biological conditions.[69] (iii) Both iron(II) and iron(III) complexes are very active in cleavage of supercoiled pUC18 plasmid DNA. The similarity in cleavage activity is expected since the presence of a large excess of DTT will force the ferric complex into a ferrous complex. Similarly, the reducing conditions in the cell will convert the Fe(III) complex into Fe(II) complex and, therefore, essentially give the same

biologically active complex involving an oxidative mechanism of action.[70,71] The cytotoxicity of all N4Py metal complexes in living cells can therefore principally be ascribed to the Fe(II)-N4Py complex.

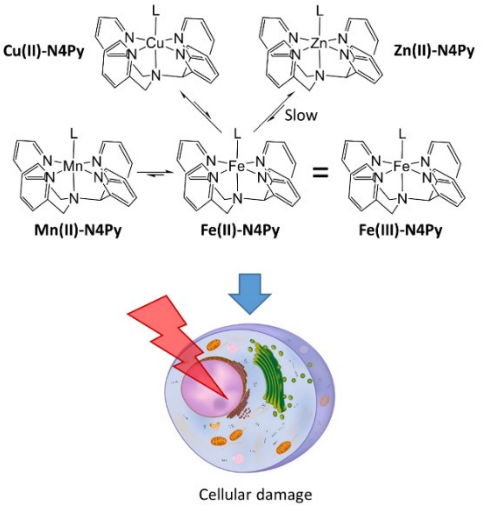

Scheme 1. Overview of the molecular processes of N4Py in the living cell.

Some apparent contradictions in the presented data seems to actually further support our hypothesis: (i) The high kinetic stability of the Zn(II)-N4Py complex is likely to account for its low cytotoxicity in the cell. Exchange with the more favored Fe(II) ion is possible, albeit limited by the slow exchange rate. In line with this, no hROS formation was observed upon treatment with Zn(II)-N4Py. The slight increase in DSBs may be accounted for by the slow exchange with Fe(II) in the N4Py complex. (ii) Cu(II)-N4Py seems to be the most preferred complex under physiological conditions, even though presence of Fe(II) can result in relatively fast formation of the Fe(II)-N4Py complex as a significant, albeit minor, species. Its lack of pUC18 plasmid DNA cleavage activity reveals the low oxidizing power of the Cu(II) complex. Generally, the cell studies with Cu(II)-N4Py resulted in little cytotoxicity to the cells at low concentrations. However, at higher concentrations, formation of the Fe(II) complex may become more evident. Conversion to the Fe(II) complex might be facilitated by reports that iron concentrations in cultured cells are often higher than copper concentrations.[72,73] (iii) The very high cytotoxicity and related high hROS levels detected for Cu(II)-N4Py in the presence of NAC, seems to be a direct result of Cu(II) interaction and complex formation with GSH to form Cu(I)-$(GSH)_2$, resulting

in strongly elevated ROS levels.[74–77] A finding that is in strong correspondence with the interaction of BLM with Cu(II) in presence of a reducing agent.[78–81]

Interestingly, the cellular damage induced by the ligand N4Py instead of its metal complexes appear to be generally even higher. We believe that this can be ascribed to additive effects: (i) Intracellular chelation of the different metals may contribute to the cytotoxicity observed for N4Py. From our competition experiments and the association/dissociation constants for the different metals as found in literature, it can be deduced that the N4Py ligand may act as a Zn(II),[35] Cu(II), and Fe(II) chelator.[34] In cells, metals often act as a co-factor in enzymatic reactions, but can also be part of a protein complex (e.g. heme proteins, iron-sulfur proteins and zinc finger proteins).[82–84] As such, they can contribute to many different cellular functions, among which apoptosis, metabolism and redox-sensing.[82] Therefore, by chelating, and, thus, scavenging metals, N4Py can influence many different cellular processes. For example, Zuo et al. have shown that Zn(II) chelation by N4Py is associated with the inhibition of the X-linked inhibitor of apoptosis (XIAP) protein.[35] By chelating Zn(II), N4Py may induce apoptosis. In another case, N4Py was shown to successfully mobilize iron from ferritin (in 5h, 5% of the total iron from ferritin is liberated),[34] the main intracellular iron storage protein.[85] This is in contrast to BLM, for which it was shown that it is unable to exchange metals with the iron storage proteins transferrin and ferritin.[79] (ii) Additionally, for reasons discussed above, the Fe(II) complex of N4Py is regarded as the main contributor to the oxidative damage that is caused to the cells. Therefore, we propose that the increased cytotoxicity of the N4Py ligand compared to the Fe(II)-N4Py complex can be ascribed to the additive effect of the intracellular chelation of metals, as well as oxidative damage. However, this study does not fully take into account the possible difference in cellular influx of the different compounds, which can have an, hitherto, unknown influence on the final concentrations in the cells.

2.4 Conclusion

In this study, it was investigated how coordination of different first row transition metals could influence the activity of the N4Py ligand in cultured cells. The outcomes of our study show that a mixture of Fe(II), Cu(II) and Zn(II) complexes can be generated when adding N4Py to cell cultures. In addition, the combination of chemical data from the analysis of N4Py metal complexes by UV/vis and cyclic voltammetry together with the performed biological assays, strongly suggest that the

active complex that causes oxidative damage to the cell is the Fe(II)-N4Py complex. The active complex can therefore differ from the complex that was initially added to the cell culture medium, regardless of the initial metal ion coordinated.

In a broader context, our study clearly shows that it is important to realize that the intracellularly active complex of a metal-coordinating compound does not always correspond to the one the cells were treated with. In view of this discrepancy, all sorts of factors have to be taken into account, including the intracellular exchange between different metals and the metal chelation by the ligand itself. Most likely it is a combination of such factors that explains the intracellular mechanism of action of such compounds. Therefore, great care has to be taken into the interpretation of the data and the conclusions that can be drawn from such studies. Therefore, in order to gain full understanding of the intracellular mode of action of coordination complexes, it is essential to combine the knowledge obtained from both chemistry and biology.

2.5 Experimental Section

2.5.1. Materials and Instrumentation

Solvents and chemicals were of reagent grade or higher and were used without any further purification. High purity water from a Millipore Milli Q purification apparatus containing a 0.22 μm filter was used. Elemental analysis was performed on a EuroVector NHCS-O Elemental Analyzer Euro EA 3000. High-resolution mass spectrometry was performed on a LTQ Orbitrap XL spectrometer. UV-Vis absorption spectra were recorded at 37°C on a Jasco V-660 spectrophotometer. The concentration of the complexes were 1 mM, unless otherwise specified, in methanol. For kinetic experiments, a SPECORD S600 diode array spectrophotometer was used. Complexes concentrations were 0.5 mM in buffer pH 7.4 and spectra were measured every 2 s over 20 min, then every 30 s. Absorption maxima are ±2 nm. Cyclic voltammetry experiments were performed using a CH Instruments potentiostat CHI600C and a 3 electrodes device (glassy carbon working electrode, Ag/AgCl reference electrode and Pt counter electrode). Voltammograms were recorded under argon from buffer solution containing 0.1 M nBu_4NPF_6, at a scan rate of 0.1 V/s and 37 °C. Concentration of complexes were 1 mM. All potential values are referred to Ag/AgCl. NMR spectra were recorded on a Varian VXR-300, Varian Mercury Plus 400 and Agilent 400-MR at 298K. Chemical shifts in ^1H spectra were internally referenced to solvent signals (^1H NMR: CD_3CN at δ = 1.94 ppm) Data are reported as follows: chemical shifts (δ), multiplicity (s = singlet, d = doublet, td = triplet of

doublets, m = multiplet), integration, and coupling constants (*J* = (Hz)).

2.5.2 Synthesis and Characterization of N4Py Metal Complexes

2.5.2.1 Synthesis

The ligand N4Py,[12,13] Fe(II)-N4Py[12,13] and Fe(III)-N4Py[26] were synthesized according to previously reported procedures. Complexation of N4Py to Mn(II), Cu(II) and Zn(II) was performed following the procedure for Fe(II)-N4Py: To a solution of 100 mg N4Py (0.27 mmol) in 1.5 mL methanol/acetonitrile 1/1 was added 1.05 eq. of $Fe(ClO_4)_2 \cdot 6H_2O$ in 1.5 mL methanol/acetonitrile 1/1. After mixing overnight, crystals suitable for X-ray crystallography were obtained by slow vapor diffusion of ethyl acetate in the methanol/acetonitrile mixture (*vide infra*). Crystals were filtered and dried on paper, and characterized by elemental analysis, absorption spectroscopy, ^{1}H-NMR and electrospray ionization mass spectrometry (ESI-MS).

$[(N4Py)Mn(CH_3CN)](ClO_4)_2 \cdot 2H_2O$ (N4Py-Mn(II)): The complex was synthesized according to previously reported procedures[44] (for complex with triflate counterion: [11,30]). The complex was isolated as white crystals after recrystallization by slow vapor diffusion of ether in a methanol/acetonitrile solution (19 %): Anal. calcd for $C_{23}H_{25}Cl_2MnN_5O_{10}$: C 42.03, H 3.83, N 10.65; found: C 42.29, H 3.45, N 10.64. UV-Vis (MeOH): λ_{max} 258 nm (ε = 13,000 $M^{-1}cm^{-1}$). HRMS: $[N4PyMnClO_4]^+$ calcd 521.066, found: 521.066; $[N4PyMnHCO_2]^+$ calcd 467.116, found: 467.115; $[N4PyMnH]^+$ calcd 423.125, found 423.125; N4Py fragments: 360.078, 328.052

$[(N4Py)Cu(CH_3CN)](ClO_4)_2 \cdot H_2O$ (N4Py-Cu(II)): The complex was synthesized according to previously reported procedures (for complex with triflate counterion:[29]). The complex was isolated as azure blue crystals after recrystallization by slow vapor diffusion of ether in a methanol/acetonitrile solution (71 %): Anal. calcd for $C_{25}H_{26}Cl_2CuN_6O_9$: C 43.58, H 3.80, N 12.20; found: C 43.54, H 3.56, N 12.07. UV-Vis (MeOH): 703 nm (ε = 80 $M^{-1}cm^{-1}$) HRMS: $[N4PyCuClO_4]^+$ calcd 529.058, found: 529.057; $[N4PyCu]^+$ calcd 430.109, found: 430.108; N4Py fragments: 337.051, 262.022

$[(N4Py)Zn(CH_3CN)](ClO_4)_2 \cdot 2H_2O$ (N4Py-Zn(II)): The complex was synthesized according to previously reported procedures (for complex with axially coordinated MeOH:[17]). The complex was isolated as pale yellow crystals after recrystallization by slow vapor diffusion of ether in a methanol/acetonitrile solution (64 %): ^{1}H NMR (400 MHz, CD_3CN) δ 4.19 (d, 2H, *J* = 18 Hz), 4.33 (d, 2H, *J* = 18 Hz), 6.02 (s, 1H), 7.18

(d, 2H, *J* = 8 Hz), 7.38-7.44 (m, 4H), 7.72-7.80 (m, 4H), 7.93 (td, 2H, *J* = 7.8 Hz, *J* = 1.7 Hz), 8.51 (d, 2H, *J* = 5.2 Hz), 8.70 (d, 2H, *J* = 5.2 Hz). Anal. calcd for $C_{23}H_{25}Cl_2ZnN_5O_{10}$: C 41.37, H 3.77, N 10.49; found: C 41.08, H 3.56, N 10.58. UV-Vis (MeOH): λ_{max} 263 nm (ε = 11,500 M^{-1} cm^{-1}). HRMS: $[N4PyZnClO_4]^+$ calcd 530.057, found: 530.056; $[N4PyZn]^+$ calcd 432.116, found: 432.116; N4Py fragments: 339.058, 273.113, 262.032

2.5.3. Analysis of X-Ray Structures of Metal-N4Py Complexes

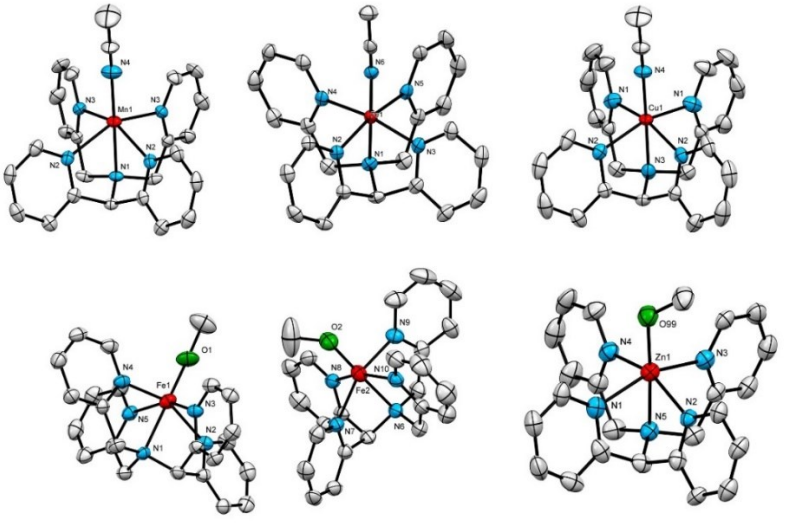

Figure S1. ORTEP plots of (a) Mn(II)-N4Py, (b) Fe(II)-N4Py, (c) Cu(II)-N4Py, (d) Fe(III)-N4Py, (e) Zn(II)-N4Py. Hydrogen atoms omitted for clarity.

Table S1. Selected Bond Lengths and Bond Angles for the Metal-N4Py Complexes

Complex:	Mn(II)-N4Py[a]	Fe(II)-N4Py[b]	Fe(III)-N4Py[c]	Fe(III)-N4Py[c]	Cu(II)-N4Py[d]	Zn(II)-N4Py[e]
M-N_{amine} (Å)	(N1) 2.262	(N1) 1.961	(N1) 2.198	(N6) 2.100	(N3) 2.154	(N5) 2.182
M-N_{py} (Å)	(N2) 2.268	(N2) 1.976	(N3) 2.115	(N8) 2.047	(N2) 2.115	(N1) 2.175
		(N3) 1.967	(N2) 2.138	(N7) 2.073		(N2) 2.227

	(N3) 2.235	(N4) 1.968	(N4) 2.105	(N9) 2.041	(N1) 2.089	(N4) 2.128
		(N5) 1.975	(N5) 2.094	(N10) 2.023		(N3) 2.117
M-$N_{acetonitrile}$ (Å)	(N4) 2.150	(N6) 1.915			(N4) 2.092	
M-$O_{methanol}$ (Å)			(O1) 1.772	(O2) 1.789		(O99) 2.032
M-$N_{py\text{-}mean\ plane}$ (Å)	0.552	0.207	0.464	0.352	0.362	0.413
(°)	(N2-Fe-N3r) 151.59	(N2-Fe-N5) 167.71	(N3-Fe-N5) 154.75	(N8-Fe-N10) 161.19	(N2-Fe-N1r) 160.15	(N1-Fe-N3) 158.41
(°)	(N1-Fe-N4) 175.91	(N1-Fe-N6) 177.32	(N1-Fe-O1) 178.97	(N6-Fe-O2) 178.55	(N3-Fe-N4) 176.17	(N5-Fe-O99) 177.18

[a] Reported in thesis of R. M. La Crois[44] and crystal structure deposited in Cambridge Crystallographic Data Centre database (CCDC). [b] Reported in [26]. [c] The Fe(III)-N4Py complex consists of two distinct $[N4PyFOMe]^{2+}$ cations in the asymmetric unit, as is consistent with its spin crossover behavior discussed in [26]. [d] X-ray structure was determined by prof. E. Otten, Stratingh institute for Chemistry, Groningen. [e] Attempts to obtain crystals suitable for X-ray analysis of Zn(II)-N4Py were unsuccessful, despite evaluating various solvents and crystallization conditions. A structural comparison of the N4Py complexes is therefore carried out with $[Zn(N4Py)(CH_3OH)](ClO_4)_2 \cdot CH_3OH$, in which the axial acetonitrile is displaced for a molecule of methanol[17].

2.5.4. Metal Binding to N4Py Under Cell-free Conditions

For simplification of the coordination studies, a few preconditions were set: 1) all reactions were performed in PBS buffer (137 mM NaCl, 2.7 mM KCl, 10 mM Na_2HPO_4, 1.8 mM KH_2PO_4) at pH 7.4, with glucose, amino acids, vitamins and phenol red being omitted from the reaction solutions, to limit competing coordination processes; 2) Due to detection limits in absorption spectroscopy and electrochemistry experiments, metal complex concentrations were generally increased to working solutions of 0.5 mM; 3) Considering that various estimations and calculations for metal concentrations in cells differ quite significantly,[72,73,86,87] it

was decided to use stoichiometric quantities in competition experiments; 4) Since ferrous iron can readily oxidize to ferric iron in the presence of oxygen, neutral or basic pH, elevated temperature (37 °C) and in presence of phosphates,[88,89] it was decided to run all experiments under anaerobic conditions.

Table S2. Details of the N4Py metal complexes obtained from the UV-vis and cyclic voltammetry spectra.

Characterization:	Fe(II)-N4Py	Fe(III)-N4Py	Cu(II)-N4Py	Mn(II)-N4Py	Zn(II)-N4Py
UV-vis: λ_{max} (ε) (nm, (cm^{-1} M^{-1}))	377 (2000) 460 (1450)	370 (> 2500)	905 (170)	320 (400)	/
CV (Epa (V))	0.06	0.05	- 0.41	0.69	/

The addition of metal ions to an N4Py solution shows the disappearance of the oxidation peak around 1.0 V vs Ag/AgCl upon binding. An example is shown in Figure S2, where upon addition of Fe(II), the appearance of a peak at 0.18 V was attributed to the (N4Py)Fe(III/II) couple. With relation to this increasing peak, the oxidation peak of N4Py at 1.0 V decreases. The disappearance of the oxidation peak can thus be correlated to the binding of metal.

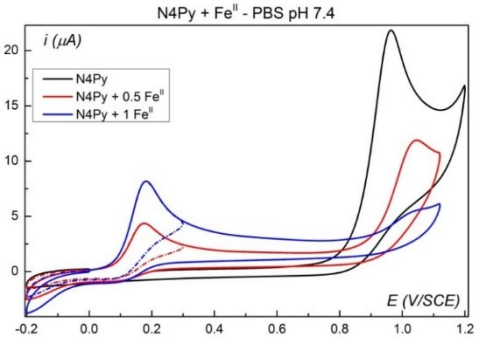

Figure S2. Cyclic voltammograms of 1 mM N4Py in PBS buffer, with addition of Fe(II).

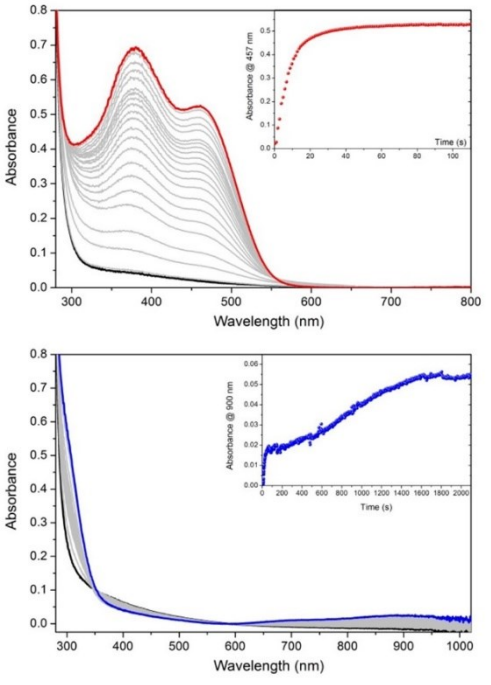

Figure S3. Absorption spectra evolution of 0.5 mM N4Py in PBS buffer in the presence of 0.5 mM Fe(II) (top) and Cu(II) (bottom). The baseline has been corrected at 700 nm for Fe(II) and 590 nm for Cu(II). Inset, time trace at 457 and 900 nm for Fe(II) and Cu(II) respectively.

Table S3. Conversion into Fe(II) and Cu(II) complexes, half-times for complex formation and rate constants.

Metals	Conversion	$t_{1/2}$	k (s^{-1})[a]
Fe(II)	74 %	15 s	0.1189
Cu(II)	50 %	30 s	0.06585

[a] rate constant determined from 2nd order-reaction fit, between 0-110 s for Fe(II) and 0-84 s for Cu(II).

Fe(II) Exchange by Transition Metal Ions

The exchange of Fe(II) by the different transition metals studied were followed by both absorption spectroscopy and cyclic voltammetry. Spectra and voltammograms of a solution containing Fe(II)-N4Py did not alter significantly over time in the presence of Fe(III), Mn(II) or Zn(II), as represented in Figure 3. In the case of Cu(II), a progressive decrease in intensity of the bands at 377 and 457 nm for the consumption of the Fe(II) complex was observed, concurrently with the formation of

a band centered at 900 nm (Figure S4, top) assigned to the Cu(II) complex. In the voltammograms, a reversible wave appeared at $E_{1/2}$ = - 0.37 V vs Ag/AgCl for the N4Py-Cu(II/I) couple (Figure S4, bottom), which correlates with the formation of the Cu(II) complex observed by absorption spectroscopy. The peak at E_{pa} = 0.06 V vs Ag/AgCl remains, which confirms the incomplete conversion of Fe(II)-N4Py into Cu(II)-N4Py.

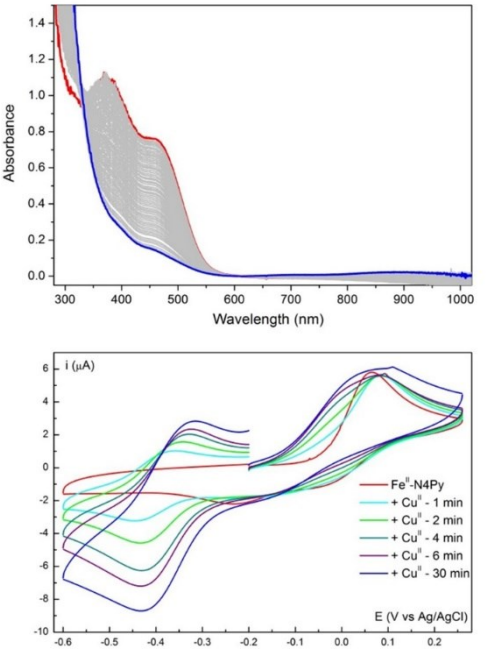

Figure S4. Top, absorption spectra evolution of 0.5 mM Fe(II)-N4Py (red) in PBS buffer in the presence of 0.5 mM Cu(II) (blue). The baseline has been corrected at 610 nm. Bottom, cyclic voltammograms evolution of the same solution, under argon.

Metal Ion Exchange by Fe(II)

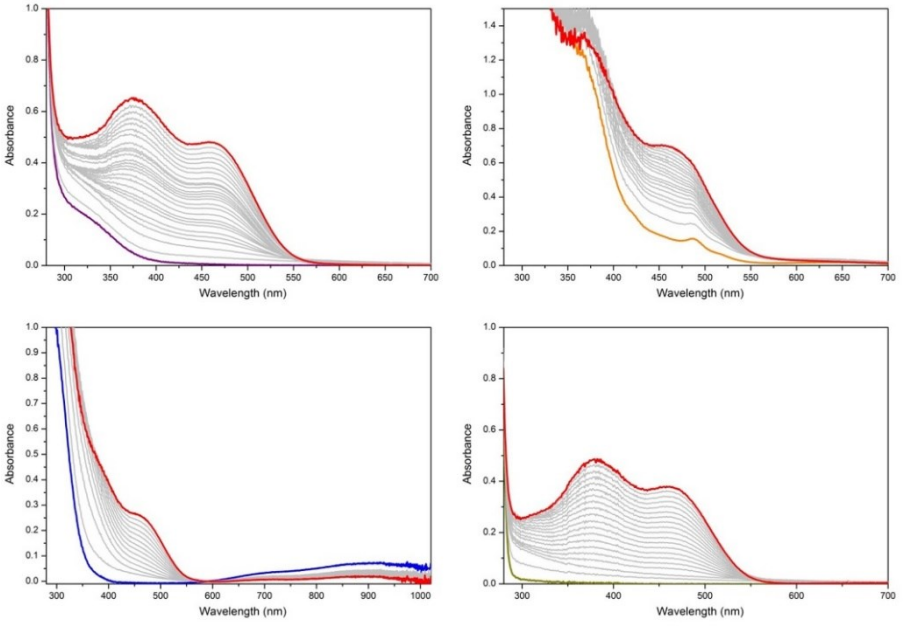

Figure S5. Absorption spectra evolution of 0.5 mM Mn(II)-N4Py (purple, left top), Fe(III)-N4Py (orange, right top), Cu(II)-N4Py (blue, left bottom) and Zn(II)-N4Py (dark yellow, right bottom) in PBS buffer in the presence of 0.5 mM Fe(II). The final spectrum is shown in red. The baseline has been corrected at 850 nm with Mn(II), Fe(III) and Zn(II), and at 590 nm with Cu(II).

2.5.5. Biological Experiments

2.5.5.1 DNA Cleavage Experiments

Materials, Instrumentation and Plasmid Isolation

pUC18 plasmid DNA, isolated from *E. coli* XL1 Blue, was purified using a QIAGEN maxi kit. Ethidium bromide (10 mg/mL in water, bioreagent) was purchased from Sigma-Aldrich. Agarose for gel electrophoresis was obtained from Sigma-Aldrich (bioreagent grade). DNA gel loading dye (6x concentrated) was purchased from Thermo Fisher Scientific. Agarose gel pictures were taken with a UVIdoc HD2 imaging system from UVITEC Cambridge. Quantification of the agarose gel bands was performed using GelQuant.NET software provided by biochemlabsolutions.com. Statistical calculations were performed using Mathematica version 9.0.0.0.

DNA Cleavage Experiments

Stock solutions of N4Py metal complexes (10 mM) were made in pure DMSO (BioReagent, Sigma-Aldrich) and diluted with Milli Q water to a final working concentration of 1 μM. The metal complexes were subsequently added to a buffered solution (Tris-HCl, 10 mM, pH 8.0) in the presence of dithiothreitol (DTT) and supercoiled pUC18 plasmid DNA in 1.5 mL Eppendorf tubes incubated at 37°C. The final reaction mixture contained a final concentration of 1.0 μM N4Py metal complex with 0.1 μg/μL DNA and 1.0 mM DTT in a total volume of 50 μL.

Samples (2 μL) were taken from the reaction solutions at t = 0 and 30 min and were directly quenched by addition to a 15 μL NaCN solution (1 mg/mL) with 3 μL loading buffer (consisting of 0.03 % bromophenol blue, 0.03 % xylene cyanol FF, 60 % glycerol, 60 mM EDTA, 6x concentrated), and immediately frozen in liquid nitrogen. The samples were run on 1.2 % agarose gels in a 1x concentrated TAE buffer for 90 minutes at 70 V. Gels were subsequently stained in an ethidium bromide bath (1.0 μg/mL) for 45 min and washed with gel running buffer. Images of the agarose gels were taken for quantification purposes and a correction factor of 1.31 was used for reduced uptake efficiency of ethidium bromide in supercoiled plasmid pUC18 DNA.[24] Results were obtained from experiments that were performed at least in triplicate.

The average number of single strand cuts per DNA molecule were calculated using Eqn. 1 (when no linear DNA is observed) or Eqn. 2 (when linear DNA is observed).[90,91] Uncertainty values for *n* were calculated by a Monte-Carlo simulation as described previously.[24,92]

(1) $f_I = e^{-n}$

(2) $f_I + f_{II} = [1 - n(2h + 1)/2L]^{n/2}$

2.5.5.2 *In vitro* Experiments

Cell Culture

The human ovarian adenocarcinoma cells A2780 and SKOV-3 were obtained from the ATCC (Manassas, VA). The temperature-sensitive, conditionally immortalized human ovarian surface epithelial cells (OSE-C2) were kindly provided by Dr. Richard Edmondson (Newcastle University, UK).[93] Cells were cultured in Dulbecco's modified Eagle's medium (DMEM) (Lonza, Verviers, Belgium) supplemented with 10 % FCS (Perbio Hyclone, Etten-Leur, The Netherlands), 50 μg/mL gentamycine sulfate (Invitrogen, Breda, The Netherlands), 2 mM L-glutamine (Lonza). A2780 and SKOV3

cells were incubated at 37 °C, and OSE-C2 cells at 33 °C in a humidified 5% CO2 incubator.

In vitro Cytotoxicity

Cell viability was measured using the MTS assay, as described previously.[33] In short, 6400 cells were seeded in 96-well plates. The next day, cells were treated with the different N4Py metal complexes, or 0.1% DMSO as a control. After 24 h, 20 µL of CellTiter 96 Aqueous One Solution (Promega, Madison, WI) was added and incubated for 3 h. The absorbance at 490 nm was measured using a Varioskan plate reader (Thermo Electron Corp., Breda, the Netherlands) and subtracted with the absorbance of cell-free medium containing reagents. Every experiment was conducted three times, and for each experiment treatments were performed in triplicate.

Cell Death (PI/FACS)

Cells were treated for 24h with the different N4Py metal complexes with or without the addition of 20 µM of the pan-caspase inhibitor zVAD-FMK. After treatment, both floating and adherent cells were harvested and stained with 5 µg/mL PI (Sigma-Aldrich)/PBS. After a 10 min incubation at 4 °C in the dark, fluorescence was measured using the FL-2 channel of a FACScalibur flow cytometer (Beckton Dickenson Biosciences, San Jose, CA). Each experiment was performed three times. The percentage PI positive cells was determined with Kaluza 1.2 (Beckman Coulter) software.

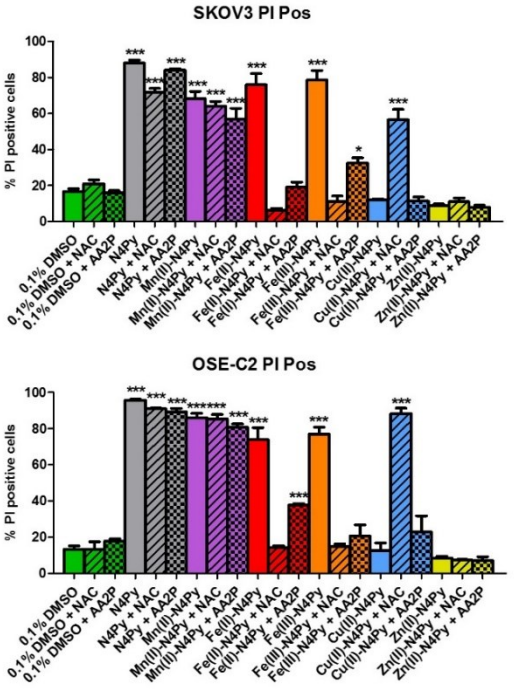

Figure S6. The effect of antioxidants on the N4Py metal complex-induced cytotoxicity. Cell death was determined in SKOV3 (top) and OSE-C2 (bottom) cells treated for 24h with 10 μM N4Py and its metal complexes (Mn(II), Fe(II), Fe(III), Cu(II), Zn(II)). Dashed and squared columns show cells co-treated with 5 μM N-acetyl cysteine (NAC) or 16h pre-treated and co-treated with 173 μM L-ascorbic acid 2-phosphate (AA2P), respectively. Cells were stained by propidium iodide and the percentage of late apoptotic/necrotic cells was analyzed by FACS. Data are presented as the mean ± SEM from three independent experiments. *** $P < 0.001$; ** $P < 0.01$; * $P < 0.05$.

dsDNA Breaks

The percentage of γH2AX positive cells (dsDNA breaks) in the healthy/early apoptotic population (subG1 population) was determined by flow cytometry as described before.[33] In short, cells were treated for 24 h and were subsequently fixed (4% formaldehyde for 10 min at 37 °C) and permeabilized (90% methanol for 30 min on ice). Cells were stained for 30 minutes at RT with a 1:50 dilution of phospho-histone H2A.X (γH2AX) (ser139) (20E3) antibody conjugated to Alexa fluor 647 (Cell Signaling, Leiden, The Netherlands). After γH2AX staining, cells were washed with PBS and stained with 5 μg/mL PI. After a 10 min incubation at 4 °C in the dark, PI fluorescence was determined in the FL2 channel, and γH2AX fluorescence was determined in the FL4 channel of a FACScalibur flow cytometer.

Cells in the subG1 population were excluded from analysis of dsDNA breaks in early/non-apoptotic cells.[94,95] The cutoff for a γH2AX positive cell was set based on a level of ~5% positivity in the solvent control. Each experiment was carried out three times. Data was analyzed with Kaluza 1.2 (Beckman Coulter) software.

ROS Detection

After a 24 h treatment with the different N4Py compounds, cells were treated with 5 µM APF (Molecular Probes) and 100 µM H_2O_2 for 30 min at 37^0C. Cells were washed with PBS and collected. APF fluorescence was detected in the FL1 channel of a flow cytometer (BD FACSCalibur, BD Biosciences). The data was analyzed with Kaluza 1.2 (Beckman Coulter) software.

Cellular Uptake

24 h after treatment, cells were visualized using a Leica DM IL microscope (Hi PLAN I 20X/0.30 PH1 lens). Photos were taken using the LAS V4.5 software (Leica Microsystems, Switzerland).

Statistics

Statistical analysis was performed using Graphpad Prism 5 software. Single group and multiple group comparisons were performed with the student's t-test or one-way ANOVA followed by Dunnett's post hoc test, respectively. A p-value of 0.05 or less was considered statistically significant.

2.6 References

(1) Umezawa, H.; Maeda, K.; Takeuchi, T.; Okami, Y. *J. Antibiot.* **1966**, *19* (5), 200.

(2) Blum, R. H.; Carter, S. K.; Agre, K. *Cancer* **1973**, *31* (4), 903.

(3) Chen, J.; Stubbe, J. *Nat. Rev. Cancer* **2005**, *5* (2), 102.

(4) Ekimoto, H.; Takahashi, K.; Matsuda, A.; Takita, T.; Umezawa, H. *J. Antibiot.* **1985**, *38* (8), 1077.

(5) Kikuchi, H.; Tetsuka, T. *J. Antibiot.* **1992**, *45* (4), 548.

(6) Rana, T. M.; Meares, C. F. *Proc. Natl. Acad. Sci.* **1991**, *88* (23), 10578.

(7) Hecht, S. M. *Bioconjug. Chem.* **1994**, *5* (6), 513.

(8) Magliozzo, R. S.; Peisach, J.; Ciriolo, M. R. *Mol. Pharmacol.* **1989**, *35* (4), 428.

(9) Stubbe, J.; Kozarich, J. W. *Chem. Rev.* **1987**, *87* (5), 1107.

(10) Young, K. J.; Takase, M. K.; Brudvig, G. W. *Inorg. Chem.* **2013**, *52* (13), 7615.

(11) Geiger, R. A.; Leto, D. F.; Chattopadhyay, S.; Dorlet, P.; Anxolabehere-

Mallart, E.; Jackson, T. A. *Inorg. Chem.* **2011**, *50* (20), 10190.
(12) Lubben, M.; Meetsma, A.; Wilkinson, E. C.; Feringa, B.; Que, L. *Angew. Chem. Int. Ed. Engl.* **1995**, *34* (13–14), 1512.
(13) Roelfes, G.; Lubben, M.; Leppard, S. W.; et al. *J. Mol. Cat. A Chem.* **1997**, *117* (1–3), 223.
(14) Draksharapu, A.; Li, Q.; Logtenberg, H.; et al. *Inorg. Chem.* **2012**, *51* (2), 900.
(15) Xie, J.; Zhou, Q.; Li, C.; Wang, W.; Hou, Y.; Zhang, B.; Wang, X. *Chem. Commun.* **2014**, *50* (49), 6520.
(16) Zhang, P.; Wang, M.; Yang, Y.; Zheng, D.; Han, K.; Sun, L. *Chem. Commun.* **2014**, *50* (91), 14153.
(17) Lo, W. K. C.; McAdam, C. J.; Blackman, A. G.; Crowley, J. D.; McMorran, D. A. *Inorg. Chim. Acta* **2015**, *426*, 183.
(18) Kojima, T.; Weber, D. M.; Choma, C. T. *Acta Crystallogr. Sect. E Struct. Reports Online* **2005**, *E60* (2), m226.
(19) Ohzu, S.; Ishizuka, T.; Hirai, Y.; Fukuzumi, S.; Kojima, T. *Chem. - Eur. J.* **2013**, *19* (5), 1563.
(20) Ohzu, S.; Ishizuka, T.; Hirai, Y.; et al. *Chem. Sci.* **2012**, *3* (12), 3421.
(21) Makino, M.; Ishizuka, T.; Ohzu, S.; Hua, J.; Kotani, H.; Kojima, T. *Inorg. Chem.* **2013**, *52* (9), 5507.
(22) Lo, W. K.; Huff, G. S.; Preston, D.; McMorran, D. A.; Giles, G. I.; Gordon, K. C.; Crowley, J. D. *Inorg. Chem.* **2015**, *54* (14), 6671.
(23) Roelfes, G.; Branum, M. E.; Wang, L.; Que Lawrence; Feringa, B. L. *J. Am. Chem. Soc.* **2000**, *122* (46), 11517.
(24) van den Berg, T. A.; Feringa, B. L.; Roelfes, G. *Chem. Commun.* **2007**, 180.
(25) Roelfes, G.; Lubben, M.; Hage, R.; Que Jr, L.; Feringa, B. L. *Chem. - Eur. J.* **2000**, *6* (12), 2152.
(26) Roelfes, G.; Lubben, M.; Chen, K.; et al. *Inorg. Chem.* **1999**, *38* (8), 1929.
(27) Roelfes, G.; Vrajmasu, V.; Chen, K.; et al. *Inorg. Chem.* **2003**, *42* (8), 2639.
(28) Ho, R. Y. N.; Roelfes, G.; Feringa, B. L.; Que, L.; Uni, V.; Tpa, L. *J. Am. Chem. Soc.* **1999**, *121* (1), 264.
(29) Kamachi, T.; Lee, Y.-M.; Nishimi, T.; Cho, J.; Yoshizawa, K.; Nam, W. *J. Phys. Chem. A* **2008**, *112* (50), 13102.
(30) Hicks, S. D.; Kim, D.; Xiong, S.; et al. *J. Am. Chem. Soc.* **2014**, *136* (9), 3680.
(31) Leto, D. F.; Ingram, R.; Day, V. W.; Jackson, T. A. *Chem. Commun.* **2013**, *49* (47), 5378.
(32) Cho, K.; Shaik, S.; Nam, W. *J. Phys. Chem. Lett.* **2012**, *3*, 2851.
(33) Li, Q.; van der Wijst, M. G.; Kazemier, H. G.; Rots, M. G.; Roelfes, G. *ACS Chem. Biol.* **2014**, *9* (4), 1044.
(34) Jackson, C. S.; Kodanko, J. J. *Metallomics* **2010**, *2* (6), 407.

(35) Zuo, J.; Schmitt, S. M.; Zhang, Z.; et al. *J. Cell. Biochem.* **2012**, *113* (8), 2567.
(36) Anderegg, G.; Hubmann, E.; Podder, N. G.; Wenk, F. *Helv. Chim. Acta* **1977**, *60* (1), 123.
(37) Hecht, S. M. *J. Nat. Prod.* **2000**, *63* (1), 158.
(38) Burger, R. M. *Chem. Rev.* **1998**, *98* (3), 1153.
(39) Sausville, E. A.; Peisach, J.; Horwitz, S. B. *Biochemistry* **1978**, *17* (14), 2740.
(40) Nagai, K.; Yamaki, H.; Suzuki, H.; Tanaka, N.; Umezawa, H. *Biochim. Biophys. Acta* **1969**, *179* (1), 165.
(41) Rao, E. A.; Saryan, L. A.; Antholine, W. E.; Petering, D. H. *J. Med. Chem.* **1980**, *23* (12), 1310.
(42) Byrnes, R. W.; Templin, J.; Sem, D.; Lyman, S.; Petering, D. H. *Cancer Res.* **1990**, *50* (17), 5275.
(43) Lyman, S.; Ujjani, B.; Renner, K.; Antholine, W.; Petering, D. H.; Whetstone, J. W.; Knight, J. M. *Cancer Res.* **1986**, *46* (9), 4472.
(44) la Crois, R. Manganese Complexes as Catalysts in Epoxidation Reactions : A Ligand Approach (dissertation), University of Groningen, 2000.
(45) Smith, J. R. L.; Masheder, D. *J. Chem. Soc. Perkin Trans. 2* **1976**, *53* (9), 47.
(46) Zweig, A.; Hodgson, W. G.; Jura, W. H. *J. Am. Chem. Soc.* **1964**, *86* (19), 4124.
(47) Irving, B. H.; Williams, R. J. P. *J. Chem. Soc.* **1953**, *637*, 3192.
(48) Slater, T. F.; Sawyer, B.; Sträuli, U. *Biochim. Biophys. Acta* **1963**, *77*, 383.
(49) Cory, A. H.; Owen, T. C.; Barltrop, J. A.; Cory, J. G. *Cancer Commun.* **1991**, *3* (7), 207.
(50) Wang, H. Z.; Chang, C. H.; Lin, C. P.; Tsai, M. C. *J. Ocul. Pharmacol. Ther.* **1996**, *12* (1), 35.
(51) Ulukaya, E.; Colakogullari, M.; Wood, E. J. *Chemotherapy* **2004**, *50* (1), 43.
(52) Wang, Y. J.; Zhou, S. M.; Xu, G.; Gao, Y. Q. *Molecules* **2015**, *20* (5), 8060.
(53) van Tonder, A.; Joubert, A. M.; Cromarty, A. D. *BMC Res. Notes* **2015**, *8*, 47.
(54) Holder, A. L.; Goth-Goldstein, R.; Lucas, D.; Koshland, C. P. *Chem. Res. Toxicol.* **2012**, *25* (9), 1885.
(55) Pozzolini, M.; Scarfi, S.; Benatti, U.; Giovine, M. *Anal. Biochem.* **2003**, *313* (2), 338.
(56) Vellonen, K. S.; Honkakoski, P.; Urtti, A. *Eur. J. Pharm. Sci.* **2004**, *23* (2), 181.
(57) Setsukinai, K. ichi; Urano, Y.; Kakinuma, K.; Majima, H. J.; Nagano, T. *J. Biol. Chem.* **2003**, *278* (5), 3170.
(58) Morley, N.; Curnow, A.; Salter, L.; Campbell, S.; Gould, D. *J. Photochem. Photobiol. Biol.* **2003**, *72* (1–3), 55.
(59) Sun, S. Y. *Cancer Biol. Ther.* **2010**, *9* (2), 109.
(60) Zafarullah, M.; Li, W. Q.; Sylvester, J.; Ahmad, M. *Cell. Mol. Life Sci.* **2003**,

60 (1), 6.

(61) Takamizawa, S.; Maehata, Y.; Imai, K.; Senoo, H.; Sato, S.; Hata, R.-I. *Cell Biol. Int.* **2004**, *28* (4), 255.

(62) Hata, R.-I.; Senoo, H. *J. Cell. Physiol.* **1989**, *138* (1), 8.

(63) Olive, P. L. *Methods Cell Biol.* **2004**, *75*, 355.

(64) Rogakou, E. P.; Boon, C.; Redon, C.; Bonner, W. M. *J. Cell Biol.* **1999**, *146* (5), 905.

(65) Takahashi, A.; Ohnishi, T. *Cancer Lett.* **2005**, *229* (2), 171.

(66) Bonner, W. M.; Redon, C. E.; Dickey, J. S.; Nakamura, A. J.; Sedelnikova, O. A.; Solier, S.; Pommier, Y. *Nat. Rev.* **2008**, *8* (12), 957.

(67) Davies, C. W.; Chaney, J.; Korbel, G.; Ringe, D.; Petsko, G. A.; Ploegh, H.; Das, C. *Bioorg. Med. Chem. Lett.* **2012**, *22* (12), 3900.

(68) Wu, X.; Seo, M. S.; Davis, K. M.; et al. *J. Am. Chem. Soc.* **2011**, *133* (50), 20088.

(69) Jacob, C.; Doering, M.; Burkholz, T. In *Redox Signaling and Regulation in Biology and Medicine*; Wiley-VCH Verlag: Weinheim, Germany; pp 63–122.

(70) Hamed, M. Y.; Silver, J.; Wilsonx, M. T. *Inorg. Chim. Acta* **1983**, *78*, 1.

(71) Hamed, M. Y.; Hider, R. C.; Silver, J. *Inorg. Chim. Acta* **1982**, *66*, 13.

(72) Wang, H.; Wang, B.; Wang, M.; et al. *Analyst* **2015**, *140* (2), 523.

(73) Parr, R. M.; Taylor, D. M. *Biochem. J.* **1964**, *91* (3), 424.

(74) Speisky, H.; Gómez, M.; Burgos-Bravo, F.; López-Alarcón, C.; Jullian, C.; Olea-Azar, C.; Aliaga, M. E. *Bioorg. Med. Chem.* **2009**, *17* (5), 1803.

(75) Speisky, H.; Gomez, M.; Carrasco-Pozo, C.; et al. *Bioorg. Med. Chem.* **2008**, *16* (13), 6568.

(76) Ueda, J.; Takai, M.; Shimazu, Y.; Ozawa, T. *Arch. Biochem. Biophys.* **1998**, *357* (2), 231.

(77) Kachur, A. V; Koch, C. J.; Biaglow, J. E. *Free Rad. Res.* **1998**, *28* (3), 259.

(78) Oppenheimer, N. J.; Chang, C.; Rodriguez, L. O.; Hecht, S. M. *J. Biol. Chem.* **1981**, *256* (4), 1514.

(79) Petering, D. H.; Byrnes, R. W.; Antholine, W. E. *Chem. Biol. Interact.* **1990**, *73* (2), 133.

(80) Ehrenfeld, G. M.; Shipley, J. B.; Heimbrook, D. C.; et al. *Biochemistry* **1987**, *26* (3), 931.

(81) Ehrenfeld, G. M.; Rodriguez, L. O.; Hecht, S. M.; Chang, C.; Basus, V. J.; Oppenheimer, N. J. *Biochemistry* **1985**, *24* (1), 81.

(82) Theil, E. C.; Raymond, K. N. *Bioinorganic Chemistry: Transition-metal storage, transport, and biomineralization*; Bertini, I., Gray, H. B., Lippard, S. J., Valentine, J. S., Eds.; University Science Books, 1994.

(83) Lill, R. *Nature* **2009**, *460* (7257), 831.

(84) Maret, W. *Adv. Nutr.* **2013**, *4* (1), 82.
(85) Ponka, P.; Beaumont, C.; Richardson, D. R. *Semin. Hematol.* **1998**, *35* (1), 35.
(86) Carpentieri, U.; Myers, J.; Thorpe, L.; Daeschner 3rd, C. W.; Haggard, M. E. *Cancer Res.* **1986**, *46* (2), 981.
(87) Kung, F. C.; Raymond, J.; Glaser, D. A. *J. Bacteriol.* **1976**, *126* (3), 1089.
(88) Faller, P.; Hureau, C.; Dorlet, P.; Hellwig, P.; Coppel, Y.; Collin, F.; Alies, B. *Met. Ions Neurodegener. Dis.* **2012**, *256* (19–20), 2381.
(89) Aslamkhan, A. G.; Aslamkhan, A.; Ahearn, G. A. *J. Exp. Zool.* **2002**, *292* (6), 507.
(90) Hertzberg, R. P.; Dervan, P. B. *J. Am. Chem. Soc.* **1982**, *104* (1), 313.
(91) Hertzberg, R. P.; Dervan, P. B. *Biochemistry* **1984**, *23* (17), 3934.
(92) Megens, R. P.; van den Berg, T. A.; de Bruijn, A. D.; Feringa, B. L.; Roelfes, G. *Chem. - Eur. J.* **2009**, *15* (7), 1723.
(93) Davies, B. R.; Steele, I. A.; Edmondson, R. J.; Zwolinski, S. A.; Saretzki, G.; von Zglinicki, T.; O'Hare, M. J. *Exp. Cell Res.* **2003**, *288* (2), 390.
(94) Darzynkiewicz, Z.; Juan, G.; Li, X.; Gorczyca, W.; Murakami, T.; Traganos, F. *Cytometry* **1997**, *27* (1), 1.
(95) Wlodkowic, D.; Skommer, J.; Darzynkiewicz, Z. *Methods Mol. Biol.* **2009**, *559*, 19.